Unidirectional compression of fibre reinforcements. Part 1: A non-linear elastic-plastic behaviour

Sébastien Comas-Cardona, Philippe Le Grognec, Christophe Binetruy, Patricia Krawczak

Unidirectional compression of fibre reinforcements. Part 1: A non-linear elastic-plastic behaviour

S. Comas-Cardona, P. Le Grognec, C. Binetruy, P. Krawczak

Polymers and Composites Technology and Mechanical Engineering Department, Ecole des Mines de Douai, 941 rue Charles Bourseul, BP 10838, 59508 Douai Cedex, France

Liquid composite moulding processes are increasingly used to manufacture composite structures. Such processes combine compres-sion of the fibre reinforcements (in dry and/or lubricated states) and resin flow. A better modelling of the compression of fibre reinforce-ments would improve the accuracy of hydro-mechanical coupling modelling involved in these processes. Several models are available in the literature, but none of them consider permanent deformations (such as plasticity). This article presents a methodology to measure plasticity of fibre reinforcements in dry and impregnated states. Also a non-linear elastic-plastic model, including large deformations, is proposed for unidirectional compression. Results on glass fibre reinforcements are presented and discussed.

Keywords: Unidirectional compression; Finite strains; A. fabrics/textiles; Elastoplasticity

1. Introduction

Structural composite materials are increasingly produced using liquid composite moulding (LCM) manufacturing techniques. During such processes, dry fibre reinforcements are placed into a rigid half mould, which is closed either with another half mould for resin transfer moulding (RTM) or with a flexible bag tooling for vacuum assisted resin transfer moulding (VARTM) for instance. The common feature between such processes is that the fibre reinforcement will be compacted. Then a flow is created to force the liquid resin through the fibre reinforcement. Positive pressure is used for RTM whereas vacuum is used during VARTM. Once the resin has impregnated the fibre reinforcements and has cured, the part can be demolded.

Two types of fibre reinforcement compressive deforma-tions can occur and be observed during processing: con-trolled and induced deformations. The deformation is qualified of "controlled" during RTM, for example, when the top half of the mould comes into close contact with the reinforcement and compresses it until reaching the desired thickness.

Induced deformations happen for most of LCM pro-cesses. During monolithic composite RTM manufacturing, the use of pressure-driven flows on dry fibre reinforcements can generate a force on the fabric surface that may deform [1]. In the case of sandwich structures manufacturing using RTM, besides the initial compression during mould closing of both core and skin reinforcements, the core can also be further compressed (e.g., deformable cores such as poly-meric foams) [2,3] and even shifted away during the filling stage [3,4]. During those processes, involving hydro-mechanical coupling, once the reinforcement is impreg-nated, it will continue to deform and eventually, when the injection is completed, it may not fully recover [3,4]. Induced deformations can also be present during processes such as VARTM. Recent studies have shown that the part thickness evolves during the resin filling. Moreover the final part thickness is not necessarily uniform and is always

Nomenclature

A	sample planar area in the deformed configuration
A_0	sample planar area in the reference configuration
C	elastoplastic compression tangent modulus of the fibre reinforcement in the z-direction
C^e	elastic compression tangent modulus of the fibre reinforcement in the z-direction
$\mathbf{E}$	Green strain tensor
$\mathbf{E^e}$	elastic strain tensor
$\mathbf{E^p}$	plastic strain tensor
$\mathrm{d}f$	force acting on a deformed area element
$\mathrm{d}\boldsymbol{f_0}$	transformed force acting on the corresponding reference area element
F	resultant force applied to the sample in the z-direction
$\mathbf{F}$	deformation gradient tensor
h	sample height in the current configuration
h_0	initial sample height
H	hardening compression modulus of the fibre reinforcement in the z-direction
$\mathbf{I}$	identity tensor
M	material point
$\mathbf{n}$	normal vector on the deformed configuration
$\mathbf{n_0}$	normal vector on the reference configuration
S	surface in the deformed configuration
S_0	surface in the reference configuration
$\mathbf{u}$	displacement
x, y, z	cartesian coordinates
α	relative shortening in the z-direction
λ	nominal stress applied to the fibre reinforcement in the z-direction
$\mathbf{\Pi}$	first Piola–Kirchhoff stress tensor
$\mathbf{\Sigma}$	second Piola–Kirchhoff stress tensor

larger at the gate than at the vent because of the mechanical equilibrium between the reinforcement stress, liquid pressure, vacuum and atmospheric pressure [5,6].

A proper modelling of the processes previously cited, especially estimating the final thicknesses of the manufactured parts, for instance, requires constitutive laws for compression of fibre reinforcements in dry and lubricated states. Such models should also take into account the different loading and unloading behaviours of the reinforcement. Numerous experimental studies have been performed for transverse compression of fibre reinforcements [7–12]. It is well known that the compression curves (pressure vs. fibre volume fraction or thickness) display a non-linear behaviour. Also, depending on the compression speed, the compression curves can be shifted revealing viscoelastic behaviour. However, Saunders et al. mentioned that, for a dry plain-woven fabric, the compression exhibits no changes with compression speeds ranging from 0.05 to 1 mm/min [11]. Also Rudd et al., working on dry glass fibre reinforcements (continuous filament random mat and quasi-unidirectional), observed that there was no significant change of compaction behaviour for compression speeds between 2 and 10 mm/min even with the presence of binder [9].

Researchers attempted to model fibre reinforcement submitted to transverse compression using power laws [8]. Other studies proposed non-linear elastic models usually based on micromechanics, where fibre bundles or fibres are assumed to behave such as elastic beams [12–14]. Those models lead to a relationship between applied pressure and fibre volume fraction and have several empirical parameters to fit to the experimental data. Other studies focused on the viscoelastic and relaxation behaviours displayed by the fibre reinforcement using a Maxwell–Wiechert viscoelastic model [15] or a non-linear viscoelastic model [16].

During VARTM, when the vacuum is initially applied to the fabrics, the latter are submitted to compression. Then, when the resin infuses the part, the fibre reinforcement is gradually unloaded. Some recent studies focused on those loading and unloading behaviours. Rudd et al. applied another compression to a sample that had already been compacted. They noted that the reinforcement did not return to its initial thickness before recompaction. They concluded that the reinforcements displayed a pseudoplastic behaviour [9]. Another study showed that elastic and permanent deformations are very significant for continuous filament random mat and plain weave fabric compressions, while viscoelasticity remains less important [17]. Also because of the limited compression speeds, involved in VARTM for instance, viscoelastic effects can be considered limited. Even though numerous previous studies focused on fibre reinforcement compression modelling, none of them seemed to include permanent deformations.

Finally, during composites manufacturing, in order to obtain the desired fibre volume fraction, the fibre reinforcements are highly compressed. A 50% reduction of the fabric thickness (between the natural thickness and the final thickness) is quite usual. Therefore, the modelling of fibre reinforcements behaviour in compression does not comply with the small strains assumption and requires the use of a large deformation formulation.

Usually during composites manufacturing, the fibre reinforcements can be compressed and sheared in the three directions of space. However, in this study we focus on the unidirectional compression behaviour in order to discard shearing effects. Therefore, a non-linear elastic-plastic constitutive law for fibre reinforcement in compressive loading and unloading including finite strains is proposed. An experimental methodology is given in order to accurately measure the model's parameters. Results of the modelling

will be given for loading and unloading of a glass fibre woven fabric in dry state to check the validity of the constitutive law.

2. Large deformation formulation

2.1. General framework

When dealing with finite deformations, i.e. strains greater than 10%, the reference and deformed states can no longer be superposed. Strains and stresses can be defined in both configurations, leading to Eulerian or Lagrangian approaches. The readers may refer to Simo and Hughes [18], for instance, for more details and fundamentals on large deformations.

Using a total Lagrangian formulation, the nominal stress $\mathbf{\Pi}$ (or first Piola–Kirchhoff stress) and the material stress $\mathbf{\Sigma}$ (or second Piola–Kirchhoff stress), which, respectively, relate forces in the current and reference configurations to areas in the reference configuration (Fig. 1), are defined as:

$$\mathrm{d}\boldsymbol{f} = \mathbf{\Pi} \cdot \mathbf{n_0} \mathrm{d}S_0 \tag{1}$$

$$\mathrm{d}\boldsymbol{f_0} = \mathbf{\Sigma} \cdot \mathbf{n_0} \mathrm{d}S_0 \tag{2}$$

The force in the reference configuration is deduced from the one in the current configuration using the suitable mapping, involving the deformation gradient, as follows:

$$\mathrm{d}\boldsymbol{f} = \mathbf{F} \cdot \mathrm{d}\boldsymbol{f_0} \tag{3}$$

which yields:

$$\mathbf{\Pi} = \mathbf{F} \cdot \mathbf{\Sigma} \tag{4}$$

The deformation is measured using the Green strain tensor $\mathbf{E}$ (energy conjugate to the second Piola–Kirchhoff stress), which can be defined in terms of the displacement $\mathbf{u}$ or the deformation gradient tensor $\mathbf{F}$:

$$\mathbf{E} = \frac{1}{2}(\nabla \mathbf{u} + \nabla^{\mathrm{T}}\mathbf{u} + \nabla^{\mathrm{T}}\mathbf{u} \cdot \nabla \mathbf{u}) = \frac{1}{2}(\mathbf{F}^{\mathrm{T}} \cdot \mathbf{F} - \mathbf{I}) \tag{5}$$

2.2. Compression between parallel platens

The constitutive law must relate the material stress $\mathbf{\Sigma}$ to the Green strain $\mathbf{E}$. Those tensors have to be expressed for the particular sample geometry and deformation involved in the considered test.

For the compression of few plies of fibre reinforcements between parallel compression platens (Fig. 2), the following assumptions can be made:

- the in-plane (x, y) deformations are neglected with respect to the through-thickness (z) deformation, because the thickness of the sample is much smaller than the diameter of the platens. Therefore, the compression can be considered unidirectional
- the compression is homogeneous within the thickness direction (z), thus the displacement field $\mathbf{u}$ can be expressed as:

$$\mathbf{u}(\mathrm{M}) = u_z \mathbf{z} = (\alpha z + \beta)\mathbf{z} \tag{6}$$

Choosing arbitrarily $u_z(0) = 0$ along with $u_z(h_0) = \Delta h$ leads to $\alpha = \Delta h / h_0$ and $\beta = 0$.

The deformation gradient tensor $\mathbf{F}$ can be expressed using the displacement field:

$$\mathbf{F} = \mathbf{I} + \nabla \mathbf{u} = \begin{bmatrix} 1 & 0 & 0 \\ 0 & 1 & 0 \\ 0 & 0 & 1+\alpha \end{bmatrix} \tag{7}$$

Using Eq. (5), the Green strain tensor becomes:

$$\mathbf{E} = \frac{1}{2}(\mathbf{F}^{\mathrm{T}} \cdot \mathbf{F} - \mathbf{I}) = \begin{bmatrix} 0 & 0 & 0 \\ 0 & 0 & 0 \\ 0 & 0 & \alpha + \frac{\alpha^2}{2} \end{bmatrix} \tag{8}$$

Let us assume a homogeneous nominal stress state within the sample:

$$\mathbf{\Pi} = \begin{bmatrix} 0 & 0 & 0 \\ 0 & 0 & 0 \\ 0 & 0 & -\lambda \end{bmatrix} \tag{9}$$

where λ is the applied pressure. The stress tensor $\mathbf{\Pi}$ verifies both equilibrium and boundary conditions.

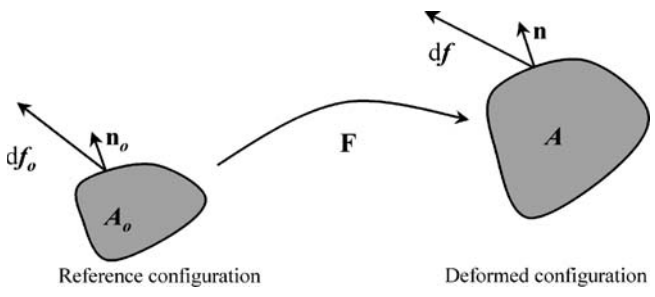

Fig. 1. Reference and deformed configurations for large deformation formulation.

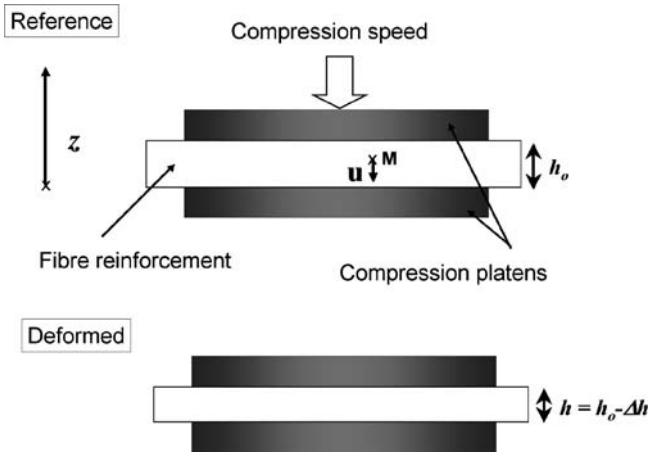

Fig. 2. Unidirectional compression geometry and displacement field.

The constitutive law involves the material stress $\mathbf{\Sigma}$ that is written:

$$\mathbf{\Sigma} = \mathbf{F}^{-1} \cdot \mathbf{\Pi} = \begin{bmatrix} 0 & 0 & 0 \\ 0 & 0 & 0 \\ 0 & 0 & -\frac{\lambda}{1+\alpha} \end{bmatrix} \tag{10}$$

3. Non-linear elastic-plastic model

3.1. Loading compression

Considering the unidirectional compression (loading step) of fibre reinforcements, in order to be consistent with the non-linear behaviour of the fibre reinforcements observed experimentally [1,8–10,15], a constitutive law that includes non-linearities must be used:

$$\mathrm{d}\Sigma_{zz} = C(E_{zz})\mathrm{d}E_{zz} \tag{11}$$

Substituting Eqs. (8) and (10) into Eq. (11) leads to:

$$\mathrm{d}\left(\frac{-\lambda}{1+\alpha}\right) = C(E_{zz})\mathrm{d}\left(\alpha + \frac{\alpha^2}{2}\right) \tag{12}$$

It can be seen from Eq. (12) that such unidirectional compression displays both material non-linearities (modulus depending on the current strain) and geometric non-linearities. The elastoplastic tangent modulus C, which has been introduced in Eq. (11), includes both elastic and plastic behaviours during the loading step.

In order to dissociate permanent deformations (plasticity) from elastic deformations during loading, the strain tensor can be additively decomposed as:

$$E_{zz} = E^{\mathrm{e}}_{zz} + E^{\mathrm{p}}_{zz} \tag{13}$$

Therefore, elastic (C^{e}) and hardening (H) moduli can be defined, such that:

$$\mathrm{d}E_{zz} = \frac{\mathrm{d}\Sigma_{zz}}{C} = \mathrm{d}E^{\mathrm{e}}_{zz} + \mathrm{d}E^{\mathrm{p}}_{zz} = \frac{\mathrm{d}\Sigma_{zz}}{C^{\mathrm{e}}} + \frac{\mathrm{d}\Sigma_{zz}}{H} \tag{14}$$

with

$$C^{\mathrm{e}} = \frac{\mathrm{d}\Sigma_{zz}}{\mathrm{d}E^{\mathrm{e}}_{zz}} \quad H = \frac{\mathrm{d}\Sigma_{zz}}{\mathrm{d}E^{p}_{zz}} \tag{15}$$

Among the unknown functions, the plastic strain $E^{\mathrm{p}}_{zz}(E_{zz})$ has to be determined. Regarding plastic strain, two approaches can be envisaged. The first one would be to model the plastic function as a superposition of several physical effects that create plasticity such as nesting, lubrication, friction... This model would be a very complete tool to predict the plastic behaviour of fibre reinforcements in compression but would also be a multi-parameter model. Generally such models are not convenient to implement in simulation tools, especially in industrial applications and environments, because of the large number of parameters involved and the difficulty to measure them. The second approach, the one retained for this study, would be a more experimental analysis using suitable compression tests to determine the plasticity of the dry and lubricated fibre reinforcements.

3.2. Unloading compression

During unloading, the behaviour is assumed to be non-linear elastic. Therefore, stress and strain are related through the following relationship:

$$\mathrm{d}\left(\frac{-\lambda}{1+\alpha}\right) = C^{\mathrm{e}}(E^{\mathrm{e}}_{zz})\mathrm{d}\left(\alpha + \frac{\alpha^2}{2}\right) \tag{16}$$

In order to find the unknown functions $C^{\mathrm{e}}(E^{\mathrm{e}}_{zz})$, $H(E_{zz})$ and $E^{\mathrm{p}}_{zz}(E_{zz})$, whether for loading or unloading steps, compression tests will be performed following procedures detailed below. Those coefficients will be measured for fibre reinforcements in dry and impregnated states.

4. Experimental setup and data analysis

Compression tests on fibre reinforcement samples are carried out on a material testing machine (Zwick). A glass twill-weave fibre reinforcement is tested (Table 1). Because of the level of stress needed to perform the compressions, a force cell of 10 kN is used.

For the compression of dry fabrics, the sample, constituted of several plies (Table 1), is inserted between two compression platens (Fig. 3). For the compression of impregnated fabrics, the setup is slightly modified. A fluid receptacle and a perforated compression platen are added (Fig. 4). The fabric, impregnated with silicone oil using a syringe for each ply, is inserted between the upper compression platen and the lower perforated platen. The combination of a low viscosity fluid, a low crosshead speed and a perforated compression platen allows to limit pressure due to the expelled liquid flow. Therefore, with those experimental setup and conditions, the measurement is limited to the mechanical response of the impregnated fabric (drained compression).

The second Piola–Kirchhoff stress (Eq. (10)) and the Green strain (Eq. (8)) are calculated using the following relations:

$$\Sigma_{zz} = \frac{-\lambda}{1+\alpha} = -\frac{F}{A_0(1+\alpha)} \tag{17}$$

$$E_{zz} = \alpha + \frac{\alpha^2}{2} \tag{18}$$

where F is the force given by the force cell and $\alpha = (h - h_0)/h_0$. The material testing machine gives the current sample height h. The initial sample height h_0 is measured with the material testing machine, when the compression force applied to the sample reaches 5 N.

Table 1
Material characteristics and experimental conditions

Areal weight	1500 g/m^2
Number of plies	4
Stacking sequence	[0°, 90°, 90°, 0°]
Initial sample height	6.8 mm
Crosshead speed	0.5 mm/min
Silicone oil viscosity (21 °C)	0.1 Pa s
Sample in-plane diameter	135 mm

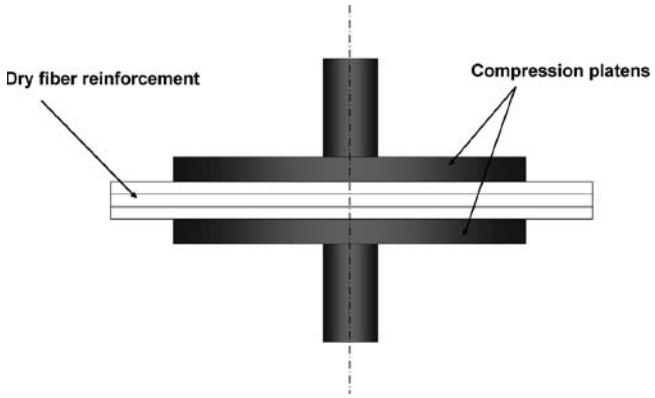

Fig. 3. Experimental setup for dry fibre reinforcement compression tests.

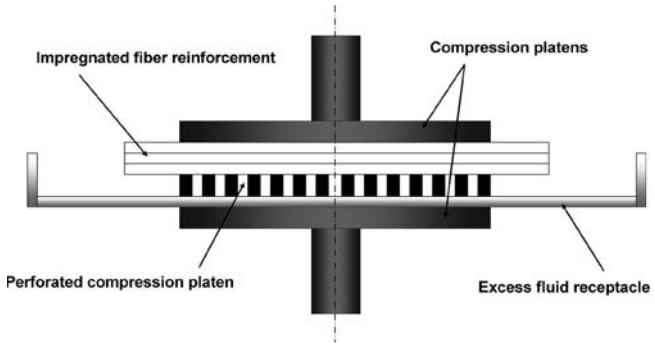

Fig. 4. Experimental setup for impregnated fibre reinforcement compression tests under drained conditions.

Since the aim of the study is to measure the fabric compression modulus including plastic effects, the compression tests are performed following two distinct procedures. First, for plasticity, the sample is loaded and subsequently unloaded. As shown in Fig. 5, the loading step deforms the sample up to a strain E_{zz}, while the unloading (down to a force of 5 N) provides the amount of permanent deformation retained in the sample E^{p}_{zz}. Each compression cycle gives a data point of the plastic strain vs. total strain curve.

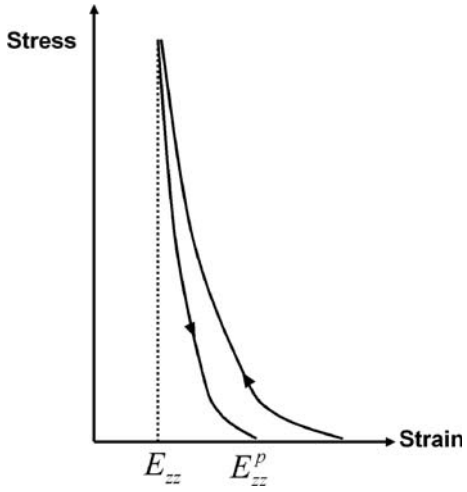

Fig. 5. Example of compression test responses that allows to extract plasticity.

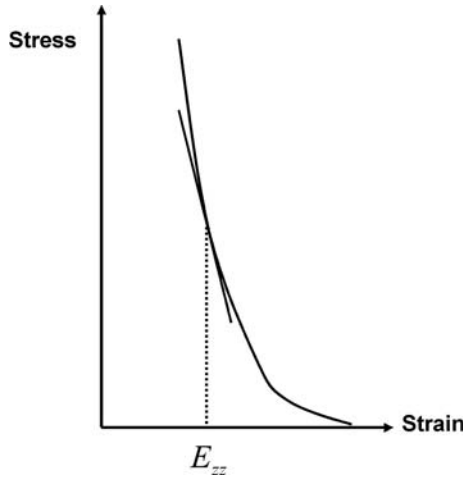

Fig. 6. Example of compression test responses that allows to extract compression modulus.

Secondly, whether the sample undergoes a loading or unloading compression test, the moduli of dry and impregnated fibre reinforcements are, respectively, taken as the local slope of the stress–strain curves (Fig. 6):

$$\Sigma_{zz} = f(E_{zz}) \tag{19}$$

5. Dry fabric results

All results presented afterwards have been obtained using a unique and low compression speed (i.e., 0.5 mm/min) in order to maintain viscoelastic effects negligible.

5.1. Compression loading and unloading

The samples are submitted to loading and unloading cycles. Fig. 7 shows the results plotted using the material stress and the Green strain as defined in Eqs. (17) and (18).

5.2. Plasticity

From the loading and unloading compression cycles, plastic strains can be extracted, following the procedure detailed previously. It can be seen in Fig. 8 that the plastic strain develops almost linearly during compression. As Somashekar et al. mentioned [17], for some fabrics in compression, most of the deformation is plastic. For the glass twill-weave fabric studied here, the plastic strain represents 70% of the total strain.

5.3. Loading compression moduli

When the fibre reinforcement is submitted to compression, it experiences elastic and plastic deformations. Using Eq. (15) and the results from Fig. 8, elastic and hardening

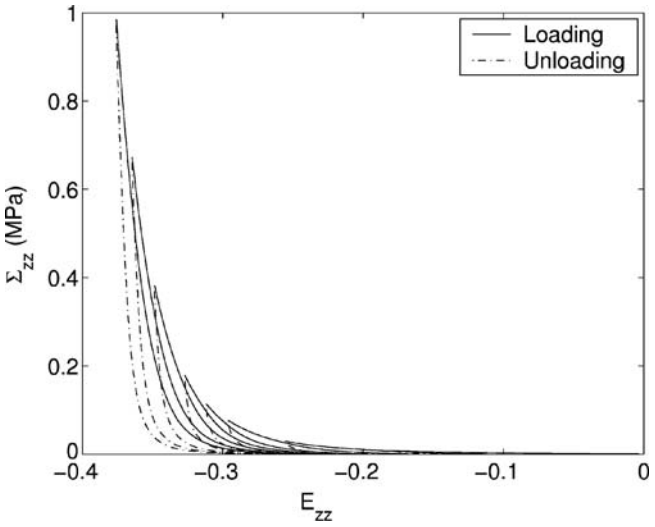

Fig. 7. Stress–strain response of the fibre reinforcement submitted to loading–unloading compressions.

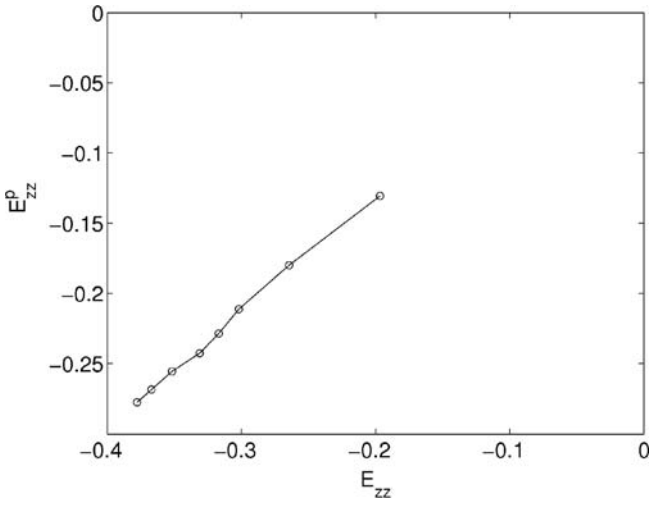

Fig. 8. Plasticity of the glass twill-weave in dry state.

moduli can be found (Fig. 9). As expected, the elastic modulus is greater than the hardening one. The non-linearity between stress and strain is confirmed here (both moduli are not constant with respect to strain).

5.4. Unloading compression modulus

If we consider that fibre reinforcements in compression behave such as non-linear elastic-plastic materials, the discharge should be fully elastic. The unloading compression moduli of the material obtained from different unloading stages are given in Fig. 10. Systematically, the unloading modulus decreases when the fibre reinforcement sample is unloaded. Using the results of compression cycles (Fig. 7) and the results of plasticity obtained in Fig. 8, the unloading (elastic) modulus curves can be plotted with respect to total strain. The unloading elastic modulus curves can also be plotted with respect to elastic strain. Such graph shows that the unloading modulus curves create a master curve

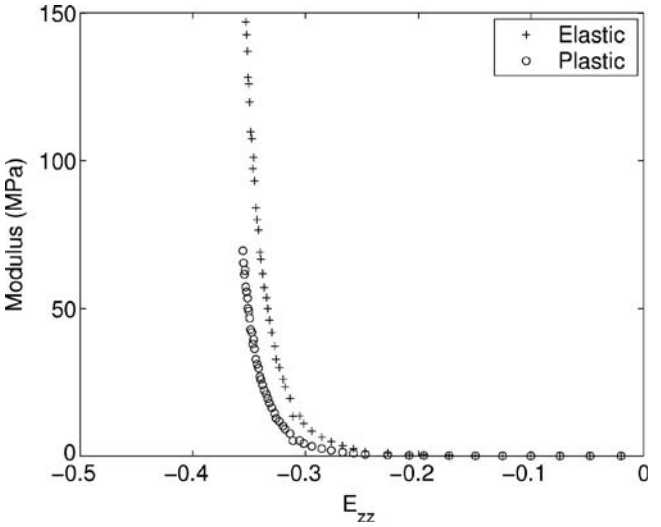

Fig. 9. Elastic (C^e) and hardening (H, plastic) compression moduli of the glass twill-weave in dry state.

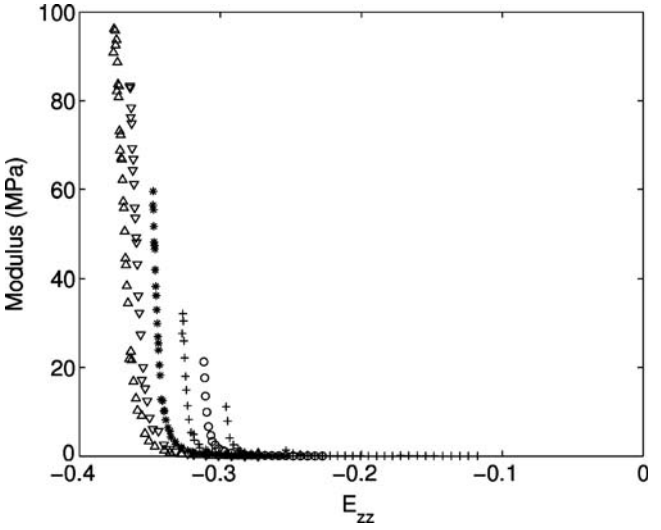

Fig. 10. Unloading compression modulus vs. total strain of the glass twill-weave in dry state.

(Fig. 11). Therefore, unloading moduli only depend on the current elastic strain whatever the level of stress reached before unloading.

5.5. Comparison between loading and unloading elastic moduli

If we consider that the dry fibre reinforcement behaves as an elasto-plastic material, the elastic moduli during loading or unloading should be equal. Fig. 12 shows that both loading and unloading elastic moduli are identical.

6. Impregnated fabric results

The plasticity is influenced by the impregnation of the fabrics as shown in Fig. 13 where both dry and impreg-

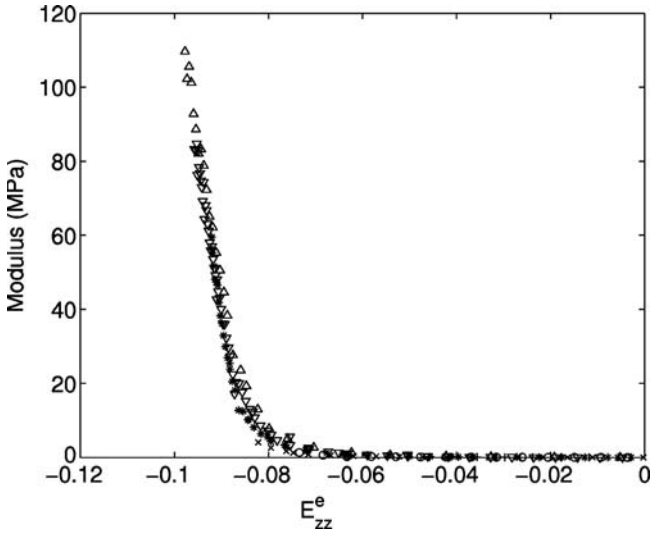

Fig. 11. Unloading compression modulus vs. elastic strain of the glass twill-weave in dry state.

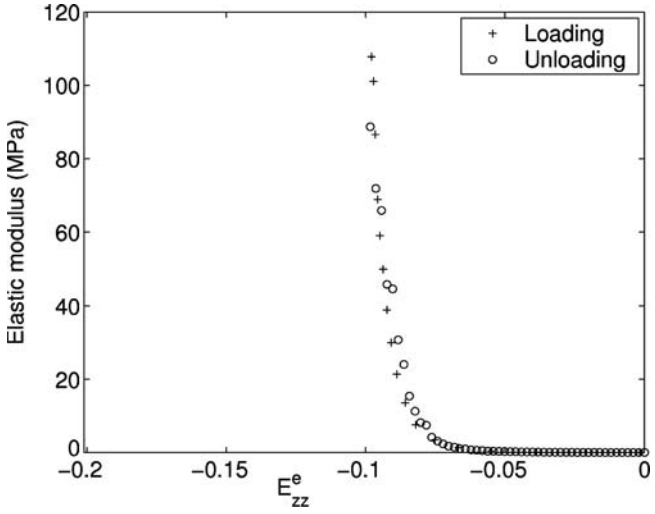

Fig. 12. Comparison of loading and unloading elastic compression moduli with respect to elastic strain.

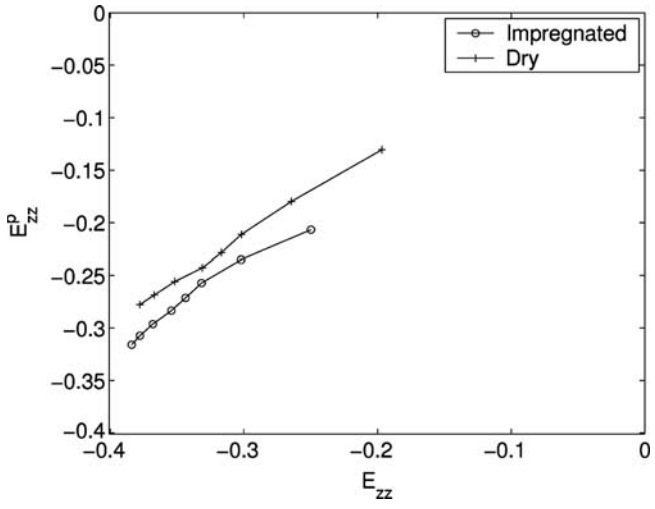

Fig. 13. Plastic strain evolution with respect to total strain for the glass twill-weave fabric in dry and impregnated states.

nated plastic strain evolution have been plotted. For such twill-weave fabric, plasticity is induced by the compression of the yarns (fibre/fibre interactions) and nesting effects (yarn/yarn interactions). The lubrication facilitates the yarn and fibre imbrications and reorganisations.

The elastic compression modulus of the dry fibre reinforcement is always greater than the one of the impregnated fibre reinforcement (Fig. 14). This effect can be explained by the presence of fluid acting as lubricating agent. The fluid helps to reduce the friction between yarns and fibres when the compression occurs. The hardening modulus is also lower for the impregnated fibre reinforcement (Fig. 15).

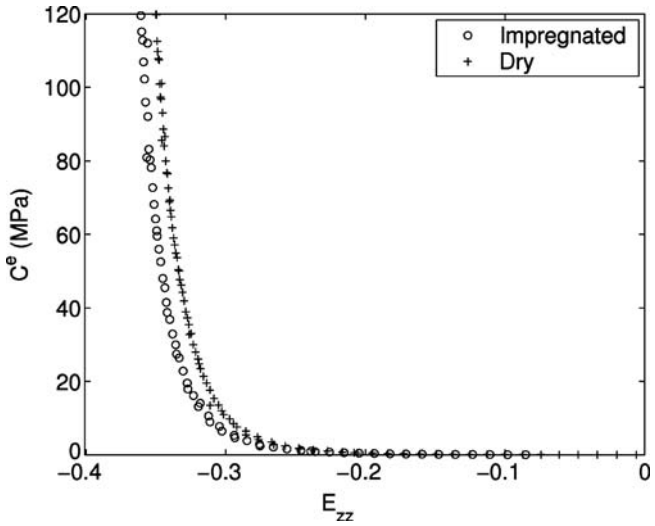

Fig. 14. Comparison of elastic compression moduli with respect to total strain for the glass twill-weave fabric in dry and impregnated states.

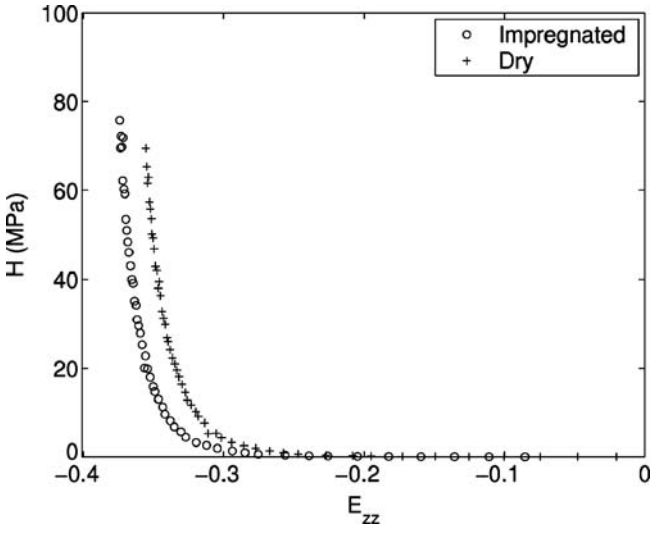

Fig. 15. Comparison of hardening compression moduli with respect to total strain for the glass twill-weave fabric in dry and impregnated states.

7. Conclusion

A simple compression setup based on a material testing machine has been proposed to test fibre reinforcements in either dry or impregnated state. As mentioned in other experimental studies [17], the results obtained for plastic strains characterisation show the importance of permanent deformations during unidirectional compression of fibre reinforcements studied here. For the twill-weave fabric studied here, the plasticity develops linearly with respect to the deformation.

In terms of compression modulus, the fluid facilitates the compaction leading to a lower compression modulus of impregnated fibre reinforcements with respect to the dry ones. This effect is due to the diminution of friction thanks to lubrication brought by the fluid.

A non-linear elastic-plastic constitutive law, using a large deformation formulation, whose parameters are measurable, has been proposed to model the behaviour of fibre reinforcements in unidirectional compression. Such model would help to better simulate composite manufacturing, especially resin infusion processes, where a fine description of fibre reinforcements in loading and unloading compression is required.

One of the assumptions made in this study was to consider that the displacement field within the thickness of the sample was linear (i.e. the deformation is homogeneous). That assumption is acceptable for rather thin samples. In the case of very thick samples, it is known that the deformation is not necessarily homogeneous and that the fabrics are more packed in the compression platen regions than at the centre of the sample. Further work would deal with that inhomogeneous displacement field for thick samples.

Also, the compression involved in this study is unidirectional. It is a limiting case of the more general 3D compression that occurs in composite manufacturing. Further work would also focus on the fact that some out-of-plane deformation (shearing) occurs when double curvature is present in preforming stages, for instance.

References

[1] Han K, Trevino L, Lee LJ, Liou M. Fibre mat deformation in liquid composite molding. I: Experimental analysis. Polym Comp 1993;14(2): 144–50.

[2] Binetruy C, Advani SG. Foam core deformation during liquid molding of sandwich structures: modeling and experimental analysis. J Sandwich Struct Mater 2003;5(4):351–76.

[3] Wirth S, Gauvin R, Kendall K. Experimental analysis of core crushing and core movements in RTM and SRIM foam cored composite parts. J Reinf Plast Comp 1998;17(11): 964–88.

[4] Al-Hamdan A, Rudd CD, Long AC. Dynamic core movement during liquid moulding of sandwich structures. Composites Part A 1998;29(3):273–82.

[5] Acheson JA, Simacek P, Advani SG. The implications of fibre compaction and saturation on fully coupled VARTM simulation. Composites Part A 2004;35(2):159–69.

[6] Tackitt KD, Walsh SM. Experimental study of thickness gradient formation in the VARTM process. Mater Manuf Process 2005;20: 607–27.

[7] Trevino L, Rupel K, Young WB. Analysis of resin injection molding in molds with replaced fiber mats I: Permeability and compressibility measurements. Polym Comp 1991;12(1):20–9.

[8] Toll S, Manson JAE. An analysis of the compressibility of fiber assemblies. In: Proceedings of the FRC Conference 1994, Newcastle upon Tyne, UK, p. 25/1–10.

[9] Rudd CD, Bulmer LJ, Morris DJ. Compaction and in-plane permeability characteristics of quasi-unidirectional and continuous random reinforcements. Mater Sci Tech 1996;12: 436–44.

[10] Robitaille F, Gauvin R. Compaction of textile reinforcements for composites manufacturing I: review of experimental results. Polym Comp 1998;19(2):198–216.

[11] Saunders RA, Lekakou C, Bader MG. Compression and microstructure of fibre plain woven cloths in the processing of polymer composites. Composites Part A 1998;29(4):443–54.

[12] Chen B, Chou TW. Compaction of woven-fabric preforms: nesting and multi-layer deformation. Comp Sci Technol 2000;60(12–13):2223–31.

[13] Lekakou C, Johari MAKB, Bader MG. Compressibility and flow permeability of two-dimensional woven reinforcements in the processing of composites. Polym Comp 1996;17(5):666–72.

[14] Batch GL, Cumiskey S, Macosko CW. Compaction of fiber reinforcements. Polym Comp 2002;23(3):307–18.

[15] Kim YR, McCarthy SP, Fanucci JP. Compressibility and relaxation of fibre reinforcements during composite processing. Polym Comp 1991;12(1):13–9.

[16] Kelly PA, Umer R, Bickerton S. Viscoelastic response of dry and wet fibrous materials during infusion processes. Composites Part A 2006;37:868–73.

[17] Somashekar AA, Bickerton S, Bhattacharyya D. An experimental investigation of non-elastic deformation of fibrous reinforcements in composites manufacturing. Composites Part A 2006;37: 858–67.

[18] Simo JC, Hughes TJR. Computational inelasticity. New York: Springer; 1998.